RESEARCH ARTICLE
doi: 10.2306/scienceasia1513-1874.2024.s004

ScienceAsia 50S (1): 2024: ID 2024s004: **1–8**

Effects of neoclassical and anomalous transport on ELM dynamics based on three-field bifurcation model

Danis Klanurak[a], Apisit Dang-iad[a], Jiraporn Promping[b], Nopporn Poolyarat[b], Siriyaporn Sangaroon[c], Apiwat Wisitsorasak[d], Ponkris Klaywittaphat[e], Boonyarit Chatthong[a,*]

[a] Division of Physical Science, Faculty of Science, Prince of Songkla University, Songkhla 90110 Thailand
[b] Thailand Institute of Nuclear Technology (Public Organization), Nakhon Nayok 26120 Thailand
[c] Department of Physics, Mahasarakham University, Maha Sarakham 44150 Thailand
[d] Department of Physics, Faculty of Science, King Mongkut's University of Technology Thonburi, Bangkok 10140 Thailand
[e] Faculty of Engineering, Thaksin University, Phatthalung 93210 Thailand

[*]Corresponding author, e-mail: boonyarit.ch@psu.ac.th

Received 26 Feb 2024, Accepted 4 Oct 2024
Available online 10 Nov 2024

ABSTRACT: The edge localized mode (ELM) instability based on peeling-ballooning models in fusion plasma is studied based on the bifurcation concept. Three field transport equations including thermal, particle, and toroidal momentum transport are numerically solved simultaneously. The transport includes both neoclassical and anomalous effects with the shearing suppression effect acting on only the anomalous channel. The total plasma current is contributed by the given driven plasma current and bootstrap current driven by local pressure gradient. An ELM is violated in the form of thermal and particle loss once either the critical pressure gradient or edge total plasma current has been reached. The ELM repetition frequency is analyzed by fast Fourier transform (FFT). The result of ELM instability exhibits a periodic fluctuation of plasma profiles as found in experiments. The energy and particle loss can be observed by the percentage drop in plasma profiles. The ELM mechanism affected by the heat source and plasma transport coefficients is examined to impose appropriate plasma conditions for avoiding deleterious ELM (type-I ELM) and creating benign ELM (type-III ELM) for tokamak devices. In addition, the percentage drop of plasma profiles is investigated by the ELM cycle.

KEYWORDS: fusion plasma, tokamak, H-mode, edge-localized-mode instability, peeling-ballooning stability model

INTRODUCTION

In many tokamak experiments, a high confinement mode (H-mode) is a success mode for plasma confinement. This mode is highly desirable because, as opposed to a low confinement mode (L-mode), the plasma yields high density, high temperature, and long energy confinement time. Experimentally, H-mode in many tokamak devices were reproduced such as ASDEX, DIII-D, and JET and on stellarators such as W7-AS [1, 2]. When the H-mode occurs, plasmas exhibit significant improvement on pressure, particle density, and temperature values. This is because in the H-mode, the plasma is more stable and better confined. Its characteristic is a sharp gradient at the plasma edge with a structure called an edge transport barrier (ETB). Top pedestal pressure is the pressure value at the top of an ETB. It is believed that the formation of ETB causes an abrupt transition from L-mode to H-mode. This transition is called an L-H transition, where anomalous transport is suppressed. The description of its mechanism is based somewhat on the shear of the radial electric field (E_r), at the onset of anomalous transport suppression and magnetic field (B), resulting in the flow shear or $E_r \times B$ in the poloidal direction [3]. The form of flow shear suppression resembles the analysis conducted by Malkov et al [4].

Experimentally, when external heating power is given to tokamak plasma. As heat flux increases, the anomalous effect gradually dominates the transport over the neoclassical, and the plasma reaches the L-mode regime. Once the heat flux surpasses a critical threshold, the plasma makes a sudden transition from L-mode to H-mode where anomalous transport is quenched in the transport barrier region. The occurrence of the L-H transition has a characteristic of a hysteresis, which can be explained using a bifurcation approach. In other words, the plasma mode can bifurcate from one regime to the other once certain criteria are satisfied [5].

In many experiments, it was found that when the plasma pressure is beyond a certain point, some instability of the plasma can be induced, which can only be detected in a short time and small length scales such as edge localized mode (ELM). ELM is a repetitive MHD instability occurring in the pedestal region in tokamak plasmas, located near the edge of the plasma inside the last closed magnetic flux surface (also known as the separatrix) in the cross-section, as shown in Fig. 1 of the previous report [6]. This instability results in energy and particle losses synchronizing with the quasi-periodic relaxation of a transport barrier previously formed during an L-H transition. This instability was first observed in the ASDEX tokamak in 1981 [7]. Experimentally, ELM instability is detected using the Visible Charged-Coupled Device Camera Diagnostic

System (Visible CCD camera). ELM can be analyzed by using the linear Magneto Hydro Dynamic (MHD) stability from the pedestal pressure and edge plasma current constraints based on the peeling-ballooning model, which has been quantitatively studied in many observations in tokamak devices [8]. There are several types of ELM instabilities observed in present tokamak devices around the world such as EAST [9], JT-60U [10], DIII-D [11], JET [12], and ASDEX Upgrade [13]. The many types of ELM that depend on the ELM violation regimes have been classified, such as type-I ELM, type-II ELM, type-III ELM, and so on [14]. Type-I ELM is a burst with a large amplitude and low repetition frequency, which appears to increase with additional heating power [9]. Type-II ELM has no clear relation on the power dependence of repetition frequency [15]. Type-III ELM is a burst with a low amplitude and high frequency, with repetition frequency decreases with increase additional heating power. Type-I ELM is one of the serious problems for tokamak devices because it releases a large power flux and can cause damage to the plasma-facing components and divertor. Type-III ELM is preferably acceptable because it has a benign power flux, which can help to expel the impurities without significantly compromising the overall energy confinement. However, type-III ELM accompanying the stationary operation in H-mode is generally found that the upper limit on the plasma pedestal is lower than that from type-I ELM, consequently reducing energy confinement. Although there is some drawback to type-III ELM, it can be neglected when considering the advantages of getting more sustainable plasma performance by clearing plasma impurities [16]. The fraction of type-I ELM energy loss to the pedestal energy ($\Delta W_{\mathrm{ELM}}/W_{\mathrm{ped}}$) is about 5%–20% and the type-III ELM has $\Delta W_{\mathrm{ELM}}/W_{\mathrm{ped}} < 5\%$ [9, 17]. Therefore, in order to avoid the large power flux from Type-I ELM, creating the acceptably transient heat loads from type-III ELM is important for tokamak devices. At present, there are several techniques based on the pedestal pressure and current control that are used to avoid the deleterious ELM and trigger the benign ELM such as pellet injection [15], resonant magnetic perturbations (RMPs) [18], plasma shaping (triangularity) control [8], and edge current density control [19]. The results of these techniques lead to the change of the ELM violation threshold based on the peeling-ballooning model, which is the key to triggering the benign ELM. Therefore, the understanding of plasma configurations to direct the appropriate ELM violation threshold for creating a benign ELM is important to tokamak devices.

This research aims to understand the ELM interaction and ELM violation regime based on peeling-ballooning models against plasma parameters using a three-field transport bifurcation model, which includes the conservation of energy, mass, and momentum. These transport equations solved in this work are based on the fluid approach model. The conservation of energy and mass has been analyzed by Chatthong et al [20] in their work to study information of both ETB and internal transport barrier (ITB). Furthermore, Gürcan et al [20–23] have extensively studied the three-field transport equations to investigate intrinsic rotation and electric field shear, among other works.

THREE-FIELD BIFURCATION MODELS

Plasma in magnetic confinement devices can be enhanced by the mechanism known as the edge of transport barrier (ETB), which occurs at the edge region of the device. ETB is formed by the suppression of plasma turbulence or anomalous transport due to the flow shear velocity. However, the existence of ETB in H-mode may bring to the occurrence of ELM instability. This research focuses on ELM instabilities that occur after the high confinement (H-mode) mode of plasma transport in magnetic confinement fusion is reached.

Three field transport equation

Effects of plasma transport on L-H transition, transport barriers formation, diffusion transport, and turbulence can be investigated using the bifurcation model. The simulations in many previous works used the bifurcation model to study and explain the dynamics or phenomena of plasma. The results from the bifurcation model are supported by theoretical understanding and data from experiments, which was confirmed by data from JET tokamak [24]. In this work, three main models of energy, mass, and toroidal momentum conservations are simultaneously solved by the calculation of transport coefficients in diffusion terms such as the critical model based on the stiffness model, which are coupled via the suppression function term [21]. Three field transport equations are shown:
Thermal transport:

$$\frac{3}{2}\frac{\partial p}{\partial t} - \frac{1}{r}\frac{\partial}{\partial r} r\left[\left(\chi_0 + \chi_1 \varepsilon\right)\frac{\partial p}{\partial r}\right] = H(r) \qquad (1)$$

Particle transport:

$$\frac{\partial n}{\partial t} - \frac{1}{r}\frac{\partial}{\partial r} r\left[\left(D_0 + D_1 \varepsilon\right)\frac{\partial n}{\partial r}\right] = S(r) \qquad (2)$$

Toroidal momentum transport:

$$n\frac{\partial v_\phi}{\partial t} - \frac{1}{r}\frac{\partial}{\partial r} rn\left[\left(v_0 + v_1 \varepsilon\right)\frac{\partial v_\phi}{\partial r} + \pi_{\mathrm{res}}\right] = \tau_\phi(r) \qquad (3)$$

where p, n and v_ϕ are plasma pressure, plasma density, and toroidal velocity, respectively; χ_0, D_0 and v_0 are the thermal, particle, and toroidal momentum neoclassical transport coefficients, respectively; χ_1, D_1 and v_1 are the thermal, particle, and toroidal momentum turbulence transport coefficients, respectively; π_{res} is

residual stress representing intrinsic torque; and ε represent the suppression function. External sources, $H(r)$, $S(r)$ and $\tau_\phi(r)$ are heat, particle and external toroidal torque sources, respectively; r is normalized radius. Gaussian's function is used to assume external sources, which includes heating, particle, and driven torque distributions into the plasma. All transport coefficients were set to be constant similar to what had been proposed [22]: $\chi_0 = 2$, $\chi_1 = 20$, $D_0 = 0.7$, $D_1 = 7$, $v_0 = 2$, $v_1 = 20$.

Critical model

The stiffness model describes the onset point of turbulence transport by using effect of sand-pile model. The relation of stiffness model is associated with radius from center of torus and gradients of pressure, density, and toroidal momentum. It can be calculated as follows [23]:
Thermal transport turbulence coefficient:

$$\chi_1^* \approx C_1 \left(\frac{R(r)}{p} \left| \frac{\partial p}{\partial r} \right| - \mu_{\nabla p} \right) \Theta \left(\frac{R(r)}{p} \frac{\partial p}{\partial r} - \mu_{\nabla p} \right) \quad (4)$$

Particle transport turbulence coefficient:

$$D_1^* \approx C_2 \left(\frac{R(r)}{n} \left| \frac{\partial n}{\partial r} \right| - \mu_{\nabla n} \right) \Theta \left(\frac{R(r)}{n} \frac{\partial n}{\partial r} - \mu_{\nabla n} \right) \quad (5)$$

Toroidal momentum transport turbulence coefficient:

$$v_1^* \approx C_3 \left(\frac{R(r)}{v_\phi} \left| \frac{\partial v_\phi}{\partial r} \right| - \mu_{\nabla v_\phi} \right) \Theta \left(\frac{R(r)}{v_\phi} \frac{\partial v_\phi}{\partial r} - \mu_{\nabla v_\phi} \right) \quad (6)$$

where C_1, C_2 and C_3 are turbulence coefficients of thermal, particle, and toroidal momentum, respectively; $\mu_{\nabla p}$, $\mu_{\nabla n}$ and $\mu_{\nabla v_\phi}$ are critical gradients of thermal, particle, and toroidal momentum, respectively; and Θ is the Heaviside function and can be defined as:

$$\Theta(\xi) = \frac{1}{2} \left(1 + \frac{\xi}{|\xi|} \right) = \begin{cases} 0, & \text{if } \xi < 0, \\ 1, & \text{if } \xi \geqslant 0. \end{cases} \quad (7)$$

Suppression function

Suppression function plays a significant role to suppress the anomalous transport from the shearing effects. Once the anomalous transport is suppressed, ETB can be formed. The suppression function affects only the turbulence term of the plasma transport coefficient in three-field plasma transport equations. In this work, two mechanisms, $E_r \times B$ shear and magnetic shear, are considered for the transport suppression function. For simplicity, the suppression function can be written as:

$$\varepsilon = \varepsilon_0 |s| \left[\left(1 + \alpha \gamma_{E\times B}^2 \right) \left(1 + \beta s^2 \right) \right]^{-1}, \quad (8)$$

where ε_0 is the coefficient suppression function; α and β are ad-hoc parameters to control the range of suppression function of flow shear and magnetic shear, respectively. Flow shear is the main mechanism for the formation of ETB, which is proportional to $E_r \times B$ velocity. The relation of flow shear can be calculated from the force balance between the gradient pressure force and Lorentz's force. The flow shear can be written in the form as shown below:

$$\gamma_{E\times B} = \frac{\partial}{\partial r} V_{E\times B} \approx -\frac{1}{B_\phi n^2} \frac{\partial p}{\partial r} \frac{\partial n}{\partial r} + \frac{B_\theta}{B_\phi} \frac{\partial v_\phi}{\partial r} + \frac{v_\phi}{B_\phi} \frac{\partial B_\theta}{\partial r} - \frac{v_\phi B_\theta}{B_\phi^2} \frac{\partial B_\phi}{\partial r} - \frac{1}{n B_\phi^2} \frac{\partial p}{\partial r} \frac{\partial B_\phi}{\partial r}, \quad (9)$$

where B_ϕ and B_θ are toroidal and poloidal magnetic field, respectively; v_ϕ and v_θ are toroidal and poloidal velocity, respectively. In experiment, turbulence can also be suppressed by magnetic topology in the plasma and forming an internal transport barrier (ITB) [25]. The definition of magnetic shear involves the parameter called safety factor, which is used to describe the twist of the magnetic field lines in the plasma. Thus, the gradient of safety factor describes the angle twist of magnetic field in different position. The magnetic shear can be written in the form of proportional of safety factor gradient as shown below:

$$s \approx \frac{r}{q} \frac{\partial q}{\partial r}, \quad (10)$$

where r and q are normalized radius and safety factor, respectively. The safety factor can be calculated as:

$$q \approx \frac{r}{R} \frac{B_\phi}{B_\theta}, \quad (11)$$

where $R(r) \sim R_0/a + r$ is a radius from center of the torus, R_0 is plasma major radius and a plasma minor radius.

Intrinsic rotation

There are several plasma phenomena, which results in the rotation in toroidal direction by plasma itself. This intrinsic rotation was studied in experiments and theory. The intrinsic rotation is important because it can drive plasma momentum in toroidal direction without the external momentum source. It is expected to be difficult to drive the momentum in larger tokamak like ITER because of its size. Intrinsic rotation can be explained using fluid and electromagnetic theory. It is caused by symmetry breaking of flow shear in radius direction. When net wave momentum is moving around the torus in asymmetrically direction by mean electric field shear, then the residual stress will be occurred. The residual stress then drives the intrinsic rotation. It can be written as [21]:

$$\pi_{\text{res}} = \kappa \varepsilon \left(1 - \sigma \frac{\partial p}{\partial r} \right) \gamma_{E\times B}, \quad (12)$$

where κ and σ are the coefficient of residual stress and ad-hoc parameter of residual stress, respectively.

Plasma current

The total plasma current is contributed by the integration of plasma current density modified as quadratics function [26] and bootstrap current density driven by the pressure gradient [20, 27]. The total plasma current is shown in the form:

$$I_p\left(r, r_{j,\text{peak}}\right) = \int_0^r \left[j_d + j_b\right] r' \, \mathrm{d}r', \qquad (13)$$

where $I_p\left(r, r_{j,\text{peak}}\right)$ is total plasma current; $j_d = j_{d,0}\left(r_{j,\text{peak}}\right)\left[1-\left(r'-r_{j,\text{peak}}\right)^2\right]^{\nu}$ is plasma current density; $j_{d,0}\left(r_{j,\text{peak}}\right)$ is a coefficient of plasma current density; $r_{j,\text{peak}}$ is position peak of driven current; j_b is the bootstrap current density, which is locally proportional to pressure gradient ($j_b \propto -\nabla p$) [28].

ELM modelling

The edge localized mode (ELM) instability in fusion plasma is studied based on peeling-ballooning models with three field transport equations including thermal, particle, and toroidal momentum transports, which are numerically solved simultaneously. This research focuses on the type-I and type-III ELM in which the peeling-ballooning ELM mechanism is simulated by setting a threshold pressure gradient and edge total plasma current. Note that other types of ELM can be caused by the condition of magnetic geometry. For instance, type-II ELM can be happened in strongly shaped plasmas at high triangularity [8, 29], however this is not included in this current work. In this research, type-I ELM and type-III ELM are triggered whenever the pressure gradient (g_p) or edge plasma current (I_p) at the ETB region exceeds the threshold ($g_p > g_{p,\text{crit}}$ or $I_p > I_{p,\text{crit}}$), respectively. Consequently, some heat and particle will be lost. Description of ELM violation modes will be describes in the next sub-section. ELM repetition frequency and the ELM loss of heat and particle are determined by referring to the typical ELM in the experiment. For instance, type-I ELM profiles are demonstrated in EAST tokamak [7, 9]. ELM heat and particle loss are demonstrated in the ELM formation of discharge from DIII-D tokamak [16]. After ELM loss, the plasma profiles are allowed to recover until another threshold is violated again, which is a characteristic of ELM cycle. The percentage drop of plasma profiles and ELM repetition frequency are investigated in this work. The percentage of plasma drop can be calculated as:

$$\%\ \text{Averaged plasma drop} = \frac{\text{Avg Max plasma} - \text{Avg Min plasma}}{\text{Avg Max plasma}} \times 100, \qquad (14)$$

where Avg Max plasma and Avg Min plasma represent the average of maximum values and average of minimum values from every oscillating cycle, respectively. Moreover, in many experiments, it is evident that there is energy and particle loss involved with the ELM repetition frequency. The ELM repetition frequency will be analyzed in the steady-state region by Fast Fourier Transform (FFT) analysis, converting the results from the spatio-temporal plasma pressure domain to the frequency domain.

ELM in pure peeling mode

The ELM in peeling mode, or type-III ELM, is defined to occur when the total plasma current exceeds a certain critical total plasma current ($I_p > I_{p,\text{crit}}$). The critical total plasma current is set to be slightly above the plasma current at the top of the pedestal in the early H-mode. When the total plasma current has reached the threshold, thermal and particles are lost by forcing reductions of their respective sources in such a way that the plasma profiles are dropped in the same fraction as observed in discharges from the DIII-D and EAST tokamaks [8, 15], specifically thermal and particles sources are reduced by around 30% for a 100 ms after which the sources are returned to its original values. Then, the plasma profiles are recovered because the thermal and particle sources are continuously supplied to the plasma until the threshold is violated again, resulting in the plasma profiles fluctuation with a certain frequency.

ELM in pure ballooning mode

The ELM in ballooning mode, or type-I ELM, is defined to occur when the pressure gradient exceeds a certain critical pressure gradient ($g_p > g_{p,\text{crit}}$). The critical pressure gradient is set to be slightly above the pressure gradient at the top of the pedestal in the early H-mode. Similarly, the thermal and particle are dropped and then increased again until the next threshold violation.

ELM in peeling-ballooning model

The peeling-ballooning model is achieved by the combination of peeling and ballooning modes from the previous section. First, both peeling and ballooning modes will be numerically solved separately in order to identify the unstable regimes. The ELM violation locations of pressure gradient and total plasma current can be observed from both data of peeling and ballooning modes. Second, unstable regimes from both simulations are combined to form a stable zone in the total plasma current versus pressure gradient coordinate. Third, two fitted equations from pure peeling and ballooning modes are then determined and then used for the violation criteria of the peeling-ballooning model. If the pressure gradient or total plasma current below the peeling-ballooning conditions, the plasma is still stable. However, when the pressure gradient or total plasma current is violated by the peeling-ballooning conditions, the ELM instability is triggered.

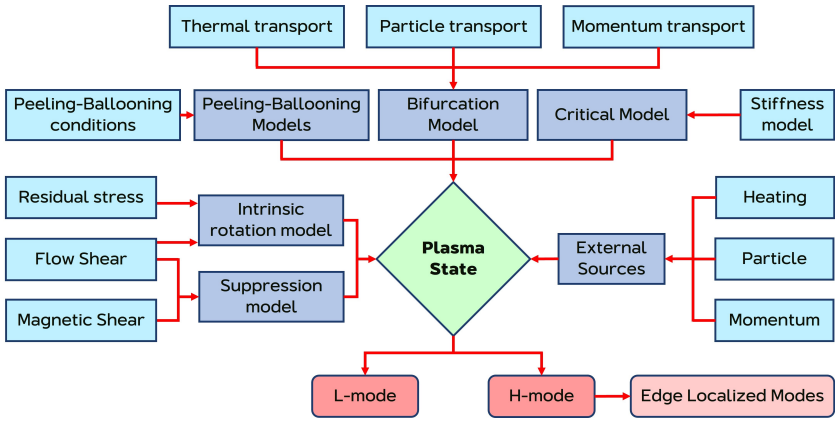

Fig. 1 Overview of the methodological framework used in this study, illustrating the processes of plasma transport, plasma state, and ELM modeling.

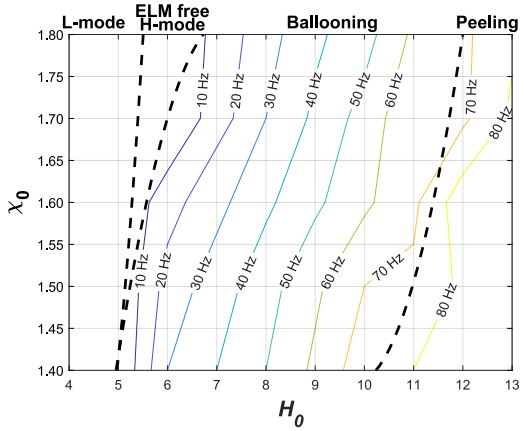

Fig. 2 Contour plots of ELM repetition frequency in peeling and ballooning modes with the x-axis as heat source coefficient (H_0) and y-axis as neoclassical thermal transport coefficient (χ_0).

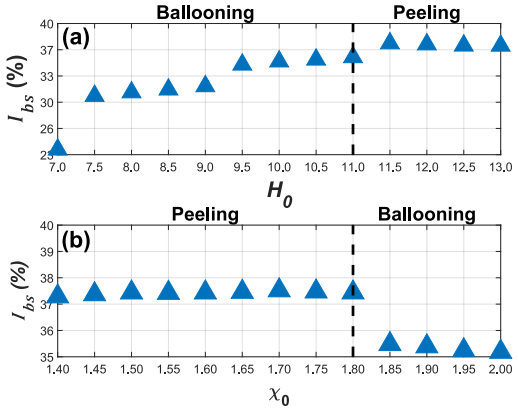

Fig. 3 Bootstrap current fraction of total plasma current $I_{\rm bs}$ (%) in peeling and ballooning modes as a function of heat source coefficient H_0 (a) and neoclassical thermal transport coefficient χ_0 (b).

Methodology diagram

The overview diagram of the method in this research, which includes plasma transport, plasma state, and ELM modeling, is depicted in Fig. 1.

RESULTS AND DISCUSSION

Investigation of ELM behaviors

This section investigates the behaviors of ELMs as the heat source coefficient (H_0) and neoclassical thermal transport coefficient (χ_0) are varied. H_0 represents the peak of plasma heating at the center based on the Gaussian function form. This represents a general source, not specific, so it could represent any scheme of external heating or plasma self-heating by fusion products. The thermal transport coefficients, both neoclassical and anomalous, physically represent the rate of plasma energy loss through diffusion, driven by coulomb collisions between plasma particles and turbulence from micro-instabilities, respectively. The ELM repetition frequency based on peeling-ballooning models is investigated in this part. The frequency of pressure fluctuation is used to indicate the ELM repetition frequency. Note that the pressure and density fluctuations caused by ELM violation yield similar frequency because it is related to both the heat and particle losses. The ELM repetition frequency appears to be increased when H_0 is increased and χ_0 is decreased. This is because, at higher H_0 and lower χ_0, the pressure gradient and flow shear are recovered faster, resulting in faster ELM violation. The ELM repetition frequency is shown as a contour field in Fig. 2 with the x-axis as H_0 and y-axis as χ_0. The three dashed lines as demonstrated in Fig. 2 separate the contour field into four regimes: L-mode; ELM free H-mode;

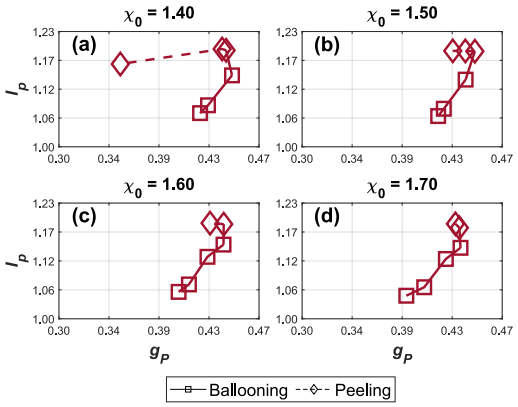

Fig. 4 ELM stability diagram when increasing heat source coefficient (H_0) at different fixed values of the neoclassical thermal transport coefficient (χ_0). The x-axis represents the pressure gradient (g_p), and the y-axis represents the total plasma current (I_p).

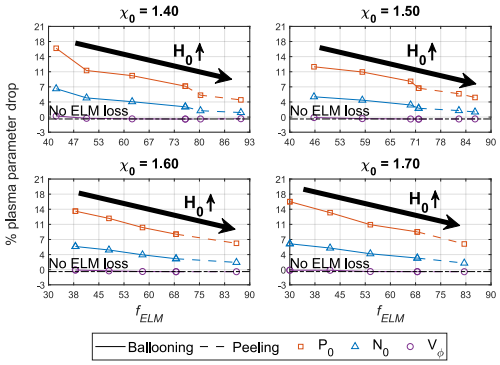

Fig. 5 Percentage drop in plasma pressure (P_0), density (N_0), and toroidal velocity (v_ϕ) when increasing heat source coefficient (H_0) at different fixed values of the neoclassical thermal transport coefficient (χ_0). The x-axis represents the ELM repetition frequency (f_{ELM}), and the y-axis represents the percentage (%) plasma parameter drop.

ELM in ballooning mode; and ELM in peeling mode. It can be seen that the characteristics of the boundary lines for χ_0 versus H_0 are rather interesting. Firstly, the L-mode regime is wider at a higher χ_0 because it requires higher to compensate the plasma loss by diffusion in order to reach the H-mode. Secondly, ELM free H-mode regime can be accessed without ELM because it is located within the peeling-ballooning stability boundary. The higher χ_0 affects the decrease of pressure gradient, allowing the plasma to easier reach the ELM in ballooning mode based on peeling-ballooning stability. However, increasing H_0 enhances the pressure gradient, leading to the onset of ELMs in the ballooning regime. Thirdly, the change of ELM violation in ballooning and peeling regimes of various χ_0 involve the influence of the edge total plasma current. ELM in peeling mode can be reached easier at the higher χ_0 because the increase of χ_0 enhance the bootstrap current. Note that the anomalous transport coefficient (χ_1) also affects ELM behaviour similar to χ_0. Moreover, the increase of H_0 also enhance the bootstrap current. Consequently, the ELM can be violated at the peeling regime at the higher H_0.

Fig. 3 shows the bootstrap current fraction, I_{bs} (%), per total plasma current versus H_0 and χ_0. The vertical dashed line separates the ELM violation from ballooning to peeling modes. It can be concluded that higher values of H_0 increases the bootstrap current, leading to the change of ELM violation from ballooning to peeling regime. However, bootstrap current is decreased at the higher χ_0, so in this case ELM violation instead changes from peeling to ballooning regimes.

The ELM violation diagram, illustrating as total plasma current (I_p) versus pressure gradient (g_p), when H_0 is varied at fixed values of χ_0 are shown in Fig. 4. The solid and dashed lines illustrate the ELM violation in ballooning and peeling boundaries, respectively. In the case of lower χ_0 ($\chi_0 = 1.40$) shown in Fig. 4, due to the influence of edge total plasma current, ELM can be violated at the peeling boundary, as opposed to the case of higher χ_0 ($\chi_0 = 1.70$), where ELM will be violated mostly at both boundaries.

Moreover, the change in the ELM violation regime results in a change in the percentage drop of plasma profiles. Examples of the percentage plasma parameters drop from simulation results of the cases in Fig. 4 are shown in Fig. 5, illustrating the percentage drops of plasma center for pressure, density, and toroidal velocity. The solid and dashed lines denote the percentage of plasma drops in ballooning and peeling boundaries, respectively. The percentage of plasma drops depends on the steepness of the ETB region, which is indicated by the pressure gradient. The percentage drops of ELM violation in the ballooning regime are higher than that of the peeling regime because the pressure gradient at ELM violation in the ballooning regime is higher than the peeling regime. When ELM is violated, the higher pressure gradient of ELM in the ballooning regime will decrease more than the peeling regime to enter the plasma stable regime again. Therefore, the percentage of plasma drops is decreased when ELM is violated in the peeling boundary because there is a lower pressure gradient. The lower percentage drop will lead to the benign ELM in the tokamak device.

Interactions of plasma profiles with ELM

The plasma profiles are influenced by the interactions of ELMs due to the limiting steepness of the ETB region. Fig. 6 depicts contour fields of plasma profiles, averaged at ELM cycle peaks during the time evolution, where the x-axis represents H_0, and the

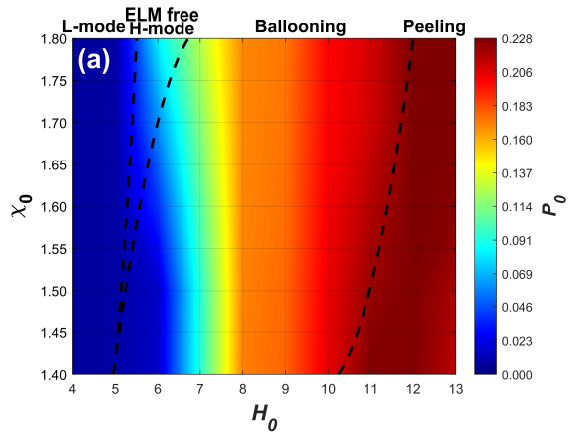

Fig. 6 Plasma profiles at the center averaged at ELM cycle peaks during the time evolution for pressure (a), density (b), and toroidal velocity (c) with the x-axis as heat source coefficient (H_0) and y-axis as neoclassical thermal transport coefficient (χ_0).

y-axis represents χ_0. There are four regimes similar to those shown in Fig. 2. The pressure (a), density (b), and toroidal velocity (c) profiles, as depicted in Fig. 6, exhibit rapid increases in L-mode and ELM-free H-mode regimes. Note that the plasma profiles at lower χ_0, as depicted in Fig. 6, grow faster than those at higher χ_0 due to the influence of the first term of flow shear (diamagnetic shear), shown in Eq. (9). Furthermore, the plasma profiles are constrained by the limitation of the ETB region when reaching the ELM in the ballooning regime, stopping their further growth. Nevertheless, considering the increased H_0, ELM can be triggered in the peeling regime. Referring to Fig. 6, the pressure and density gradually decrease due to the lower steepness of the ETB region when reaching the ELM in the peeling regime. However, since the toroidal velocity is not directly impacted by the ELM, but depends mainly on density and U_0, leading to an increase in velocity despite ELM violations in the peeling mode.

CONCLUSION

The edge localized mode (ELM) instability based on peeling-ballooning models has been studied by using three-field transport equations, which consist of thermal, particle, and toroidal momentum transport. The ELM interactions are investigated by neoclassical thermal transport coefficient (χ_0). The increase of H_0 affects the ELM repetition frequency enhancement because the flow shear can be recovered faster at the higher H_0, leading to higher frequency ELM. ELM can be controlled by controlling H_0. Increasing χ_0 leads to a reduction in the edge total plasma current contributed by the bootstrap current, consequently elevating the probability of type-I ELM occurrence in the ballooning regime. This results in the plasma pressure and density reaching their highest levels due to the highest steepness of the ETB region, accompanied by a significant loss of ELM energy. Furthermore, in the peeling regime, the probability of type-III ELM occurrence increases with the decreasing χ_0 due to an elevated edge total plasma current. Furthermore, the anomalous transport coefficient (χ_1) causes similar effects as χ_0 on plasma and ELMs. Particle and momentum transport coefficients, however, do not have a similar effect on plasma due to their low sensitivity to pressure gradient and bootstrap current. The plasma pressure and density decrease due to the lower steepness of the ETB region, accompanied by a reduction in ELM energy loss. On the other hand, toroidal velocity continues to rise in both ELM peeling and ballooning regimes since it is not directly impacted by the ELM but depends mainly on density and U_0. Although type-III ELMs exhibit lower plasma pressure and density, this drawback can be compensated by the reduced ELM energy loss, resulting in a more benign impact on the wall of the tokamak device.

Acknowledgements: This research was partially supported by Program Management Unit for Human Resources and Institutional Development, Research and Innovation fiscal year 2023, grant number B39G670014 and the Thailand Science Research and Innovation (TSRI) Fundamental Fund FY2566 (Project Number 4369603). D. Klanurak thanks his graduate scholarship from Faculty of Science Research Fund, Prince of Songkla University, Contract no. 1-2564-02-004. B. Chatthong acknowledges TINT to University Program.

REFERENCES

1. Hugill J (2000) Edge turbulence in tokamaks and the L-mode to H-mode transition. *Plasma Phys Control Fusion* **42**, R75.
2. Erckmann V, Wagner F, Baldzuhn J, Brakel R, Burhenn R, Gasparino U, Grigull P, Hartfuss HJ, et al (1993) H mode of the W 7-AS stellarator. *Phys Rev Lett* **70**, 2086–2089.
3. Burrell KH (1997) Effects of $E \times B$ velocity shear and magnetic shear on turbulence and transport in magnetic confinement devices. *Phys Plasmas* **4**, 1499–1518.
4. Malkov MA, Diamond PH (2008) Analytic theory of L-H transition, barrier structure, and hysteresis for a simple model of coupled particle and heat fluxes. *Phys Plasmas* **15**, 122301.
5. Chatthong B, Onjun T (2017) Formation and sustainability of H-mode regime in tokamak plasma via sources perturbations based on two-field bifurcation concept. *Sains Malays* **46**, 1385–1392.
6. Costea S, Tskhakaya D, Kovačič J, Gyergyek T, Schrittwieser R, Ionita C, Schneider B, et al (2021) Particle-In-Cell simulation of parallel blob dynamics in near scrape-off-layer plasma of medium-size tokamak. *Plasma Phys Control Fusion* **63**, 055016.
7. Wagner F, Becker G, Behringer K, Campbell D, Eberhagen A, Engelhardt W, Fussmann G, Gehre O, et al (1982) Regime of improved confinement and high beta

in neutral-beam-heated divertor discharges of the ASDEX tokamak. *Phys Rev Lett* **49**, 1408–1412.
8. Snyder PB, Burrell KH, Wilson HR, Chu MS, Fenstermacher ME, Leonard AW, Moyer RA, Osborne TH, et al (2007) Stability and dynamics of the edge pedestal in the low collisionality regime: physics mechanisms for steady-state ELM-free operation. *Nucl Fusion* **47**, 961.
9. Chen S, Zhong F, Yang Q, Li L, Liang Y, Zhang B, Hu L (2019) Parametric dependence of type-I and type-III ELMs and dynamic characteristics for ELM filaments in EAST tokamak. *IEEE Trans Plasma Sci* **47**, 799–806.
10. Oyama N, Sakamoto Y, Isayama A, Takechi M, Gohil P, Lao LL, Snyder PB, Fujita T, et al (2005) Energy loss for grassy ELMs and effects of plasma rotation on the ELM characteristics in JT-60U. *Nucl Fusion* **45**, 871.
11. Burrell KH, Austin ME, Brennan DP, DeBoo JC, Doyle EJ, Gohil P, Greenfield CM, Groebner RJ, et al (2002) Quiescent H-mode plasmas in the DIII-D tokamak. *Plasma Phys Control Fusion* **44**, A253.
12. Garcia J, de la Luna E, Sertoli M, Casson FJ, Mazzi S, Štancar Ž, Szepesi G, Frigione D, et al (2022) New H-mode regimes with small ELMs and high thermal confinement in the Joint European Torus. *Phys Plasmas* **29**, 032505.
13. Harrer GF, Faitsch M, Radovanovic L, Wolfrum E, Albert C, Cathey A, Cavedon M, Dunne M, et al (2022) Quasicontinuous exhaust scenario for a fusion reactor: The renaissance of small edge localized modes. *Phys Rev Lett* **129**, 165001.
14. Wilson H (2010) Edge localized modes in tokamaks. *Fusion Sci Technol* **57**, 174–182.
15. Hou J, Hu J, Chen Y, Wang Y, Zang Q, Xu J, Liu H, Tritz K, et al (2019) Deuterium pellet fueling in type-III ELMy H-mode plasmas on EAST superconducting tokamak. *Fusion Eng Des* **145**, 79–86.
16. Leonard AW (2014) Edge-localized-modes in tokamaksa. *Phys Plasmas* **21**, 090501.
17. Hill DN (1997) A review of ELMs in divertor tokamaks. *J Nucl Mater* **241–243**, 182–198.
18. Suttrop W, Kirk A, Bobkov V, Cavedon M, Dunne M, McDermott RM, Meyer H, Nazikian R, et al (2018) Experimental conditions to suppress edge localised modes by magnetic perturbations in the ASDEX Upgrade tokamak. *Nucl Fusion* **58**, 096031.
19. Becoulet M, Huysmans G, Thomas P, Joffrin E, Rimini F, Monier-Garbet P, Grosman A, Ghendrih P, et al (2005) Edge localized modes control: experiment and theory. *J Nucl Mater* **337–339**, 677–683.
20. Chatthong B, Onjun T (2016) Understanding roles of $E \times B$ flow and magnetic shear on the formation of internal and edge transport barriers using two-field bifurcation concept. *Nucl Fusion* **56**, 016010.
21. Gürcan ÖD, Diamond PH, Hahm TS, Singh R (2007) Intrinsic rotation and electric field shear. *Phys Plasmas* **14**, 042306.
22. Gürcan ÖD, Diamond PH, McDevitt CJ, Hahm TS (2010) A simple model of intrinsic rotation in high confinement regime tokamak plasmas. *Phys Plasmas* **17**, 032509.
23. Garbet X, Mantica P, Ryter F, Cordey G, Imbeaux F, Sozzi C, Manini A, Asp E, et al (2004) Profile stiffness and global confinement. *Plasma Phys Control Fusion* **46**, 1351.
24. Bak P, Balet B, Cherubini A, Cordey JG, Deliyanakis N, Erba M, Parail VV, Forte L, et al (1996) Physics of L and H mode confinement in JET. *Nucl Fusion* **36**, 321.
25. Koide Y, Takizuka T, Takeji S, Ishida S, Kikuchi M, Kamada Y, Ozeki T, Neyatani Y, et al (1996) Internal transport barrier with improved confinement in the JT-60U tokamak. *Plasma Phys Control Fusion* **38**, 1011.
26. Cairns RA (2005) *Tokamaks*, 3rd edn, Oxford University Press, Oxford, United Kingdom.
27. Andrade MCR, Ludwig GO (2008) Scaling of bootstrap current on equilibrium and plasma profile parameters in tokamak plasmas. *Plasma Phys Control Fusion* **50**, 065001.
28. Gott YV, Yurchenko ÉI (2002) Physical nature of the electric current produced by the asymmetry of particle motion in toroidal magnetic confinement systems. *Plasma Phys Rep* **28**, 382–394.
29. Coda S, Porkolab M, Burrell KH (2001) Characterization of density fluctuations during ELMs in the DIII-D tokamak. *Nucl Fusion* **41**, 1885.